Optical Properties of Fluid Hydrogen at the Transition to a Conducting State

R. Stewart McWilliams,[1,2,3,*] D. Allen Dalton,[1] Mohammad F. Mahmood,[1,3] and Alexander F. Goncharov[1,4,5,†]
[1]Geophysical Laboratory, Carnegie Institution of Washington, 5251 Broad Branch Road NW, Washington D.C. 20015, USA
[2]School of Physics and Astronomy and Centre for Science at Extreme Conditions, University of Edinburgh, Peter Guthrie Tait Road, Edinburgh, United Kingdom EH9 3FD
[3]Department of Mathematics, Howard University, 2400 Sixth Street NW, Washington D.C. 20059, USA
[4]Key Laboratory of Materials Physics, Institute of Solid State Physics, Chinese Academy of Sciences, 350 Shushanghu Road, Hefei, Anhui 230031, China
[5]University of Science and Technology of China, Hefei, Anhui 230026, China
(Received 21 July 2015; revised manuscript received 29 January 2016; published 22 June 2016)

We use fast transient transmission and emission spectroscopies in the pulse laser heated diamond anvil cell to probe the energy-dependent optical properties of hydrogen at pressures of 10–150 GPa and temperatures up to 6000 K. Hydrogen is absorptive at visible to near-infrared wavelengths above a threshold temperature that decreases from 3000 K at 18 GPa to 1700 K at 110 GPa. Transmission spectra at 2400 K and 141 GPa indicate that the absorptive hydrogen is semiconducting or semimetallic in character, definitively ruling out a first-order insulator-metal transition in the studied pressure range.

DOI: 10.1103/PhysRevLett.116.255501

Realizing metallic hydrogen and understanding its properties is fundamental for achieving predicted high-temperature superconductivity [1], exploring the regime of inertial confinement fusion [2], and resolving the structure and dynamics of giant planetary interiors [3–7]. The metallic state has not been reached in the solid at pressures as high as 360 GPa [8–10], but experiments [3,11–16] and theoretical calculations [5,16–27] probing the fluid state at high temperature document an insulator-metal transition (IMT). This fluid metallic state has been theorized to be even the ground state at sufficiently high pressures [19,20]; however, recent experiments suggest more complex behavior [16,28].

While the underlying physics of metallization in hydrogen is thought to be related to a Mott-like mechanism (band overlap), the essential parts of this phenomenon remain uncaptured because of difficulties in finding appropriate theoretical approximation methods [25–27] and experimental challenges. With increasing pressure, the fluid IMT is expected to exhibit a *critical point,* where it transitions from being continuous to discontinuous (first order), and merge with the melting line in the limit of high densities [19,20]. Different theoretical studies agree about the transition character, but the location of the critical point varies substantially, with modern estimates ranging as low as 90 GPa [4,5,19,21,22,25–27].

Experiments on fluid hydrogen using shock compression measured gradual increases in electrical conductivity and optical reflectivity to constant, metallic values with increasing temperature and pressure up to 90 GPa [11,13,14], evincing a continuous IMT below this pressure. Between 90 and 140 GPa shock experiments were conducted without direct temperature measurements, such that the gradual increase and saturation of conductivity detected in this region [3,12,29] is open to interpretation: the data are consistent with a continuous IMT [3,12,29] but also show characteristics of a first-order IMT naturally broadened by adiabatic compression (see, e.g., Ref. [30]). Recent isentropic compression measurements suggest the IMT becomes first order by 285 GPa [16], but also assumed temperature, leaving a broad pressure range [3,12,16,29] where the nature of the IMT remains incompletely characterized. Static compression, diamond anvil cell experiments demonstrated direct temperature measurements in the metallization regime at high pressure, and detected a fluid phase transition at ~120 GPa, though were not able to provide any characteristics of the transformed state [15].

Hydrogen is challenging to contain in high-temperature and high-pressure experiments for long periods owing to its high reactivity and diffusivity [28,31]. Dynamic compression has probed hydrogen beyond several thousand degrees kelvin at high pressures in experiments on microsecond or faster time scales [3,11–14,29], whereas static diamond cell experiments using resistive [28] and laser heating [15,31,32] on cumulatively longer time scales reached 1000 K and 1800 K, respectively.

In this Letter we describe microsecond, single-pulse laser heated diamond cell experiments on hydrogen that reach novel high-temperature conditions not previously characterized by dynamic or static studies (Fig. 1). Time-resolved optical emission and transmission spectroscopy determines sample temperature T and corresponding optical absorptivity α during heat cycles [34,38]. A 4–10 μs long laser pulse heats a metallic (Ir) foil in a hydrogen sample, and heat propagates across the adjacent hydrogen creating a localized heated excited state of several μm in linear dimensions and a few μs long. Transient absorption probing using a continuous laser (cw, 532 nm) and pulsed broadband supercontinuum (BB, 1 MHz, 150 ps, 400–900 nm) was performed by transmission through a hole in the foil at the heated region. Fits of emission spectra to a Planck distribution determined temperature with a time resolution of 0.5–5 μs.

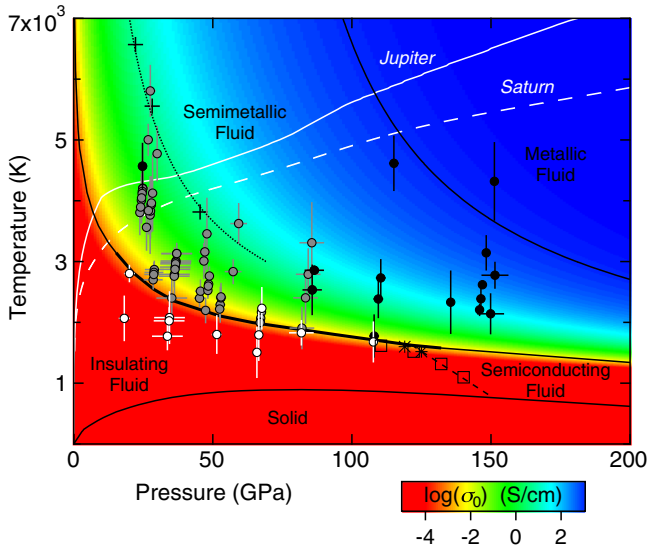

FIG. 1. Phase diagram of hydrogen. Black lines are phase boundaries. Present measurements are filled circles for transparent (white) and absorbing (gray, black) hydrogen; black points are characterized via direct transient absorption measurement (Fig. 2), whereas gray points correspond to anomalous temperature responses observed upon increasing heating laser power (Fig. 3). A thermal pressure of 2.5 GPa/1000 K [33] is included. The heavy black line is the onset of absorbing hydrogen in the present data. Prior measurements are the onset of reflectivity in shock compression [14] (crosses and dotted line), the onset of visible absorption in isentropic compression [16] (squares and dashed line), the location of anomalies in temperature with increasing heating laser power in the diamond cell [15] (stars), and the dc conductivity (color map) based on interpolated data [3,11,12,29,34,35]. The melting curve is taken from Ref. [28], and the metallization line is the saturation of dc conductivity. White lines are interior conditions of Jupiter [36] and Saturn [37].

To ensure our measurements probed pristine hydrogen, several precautions were taken. Pressure was measured before and after the heat cycles using Raman spectra of the hydrogen vibron [39] and diamond edge [40] and ruby fluorescence [41]. The vibron signal from the heated area was confirmed before and after heating [34]. Continued heating resulted in decreasing vibron signal, pressure changes (usually but not always negative), decreasing foil hole diameters [34], and occasional anvil fracturing, evincing rapid hydrogen diffusion and loss. Complete loss occurred within ~1 ms of total heating time. Weak Raman lines attributed to Ir hydride [42] appeared in one sample subjected to prolonged heating at high temperature [34], but not in reported experiments.

Upon increasing laser power, time histories of thermal emission during heat cycles exhibited a drastic shift in behavior, similar to that seen in noble gases as a consequence of high-temperature absorption onset [38]. For low peak laser power, the temperature followed the laser power history [Fig. 2(a)], having a distinct initial peak. With increasing power, there was a transition to a different thermal response, where temperature did not follow laser power, but instead rose and remained roughly constant, forming a plateau that persisted for an especially long duration (Fig. 3). To examine this transition we performed finite element (FE) models [34,38,43] to investigate how properties of hydrogen samples, such as a temperature-dependent absorption, control temperature history. The lower-temperature behavior is expected for a transparent sample, i.e., where the laser is absorbed entirely in the foil surface. The higher-temperature behavior could not be explained if the sample remained transparent; instead, an abrupt increase in sample absorption with temperature (to $\alpha \approx 0.1$–$1\ \mu m^{-1}$) is needed to reproduce the long temperature plateau, which occurs near the temperature of

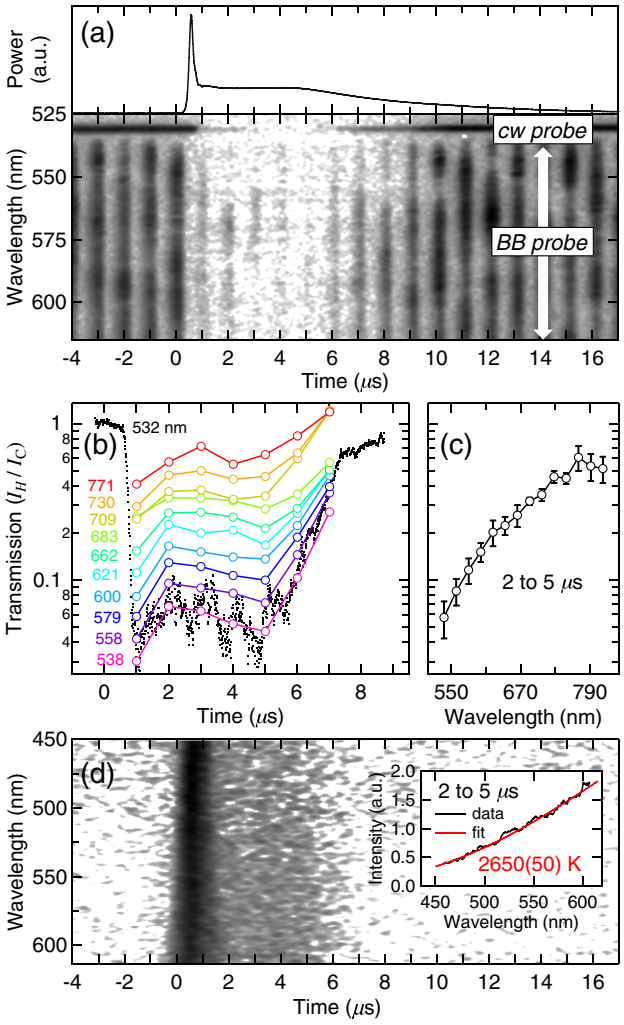

FIG. 2. Transient absorption and emission measurements in hydrogen at 141 GPa. (a) Laser power (upper panel) and spectrogram showing transient absorption (lower panel). (b) Time histories of absorption at different wavelengths using pulse referencing [34,38]. (c) Transmission spectrum averaged over 2–5 μs where absorption (and temperature) is roughly constant. (d) Emission spectrogram (20 spectrograms stacked), with inset showing graybody Planck fit to data at 2–5 μs. Temperature in this time interval was 2400(300) in a series of heat cycles at this laser power. Arbitrary units are a.u.

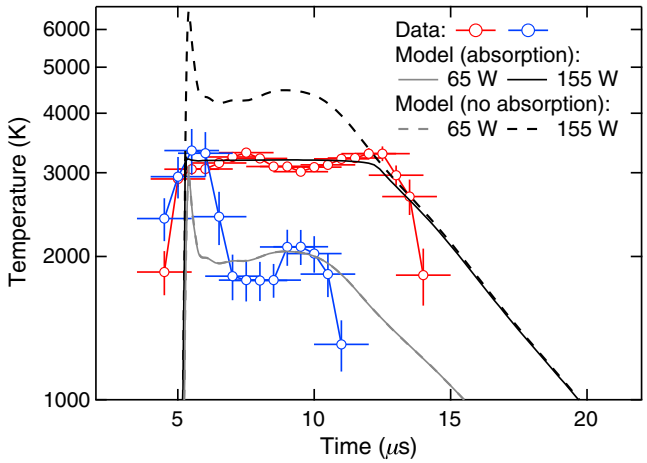

FIG. 3. Temperature histories at 30 GPa with finite element model predictions. Two measurements (open symbols: vertical bars are temperature uncertainty, horizontal bars are time resolution) are presented with finite element models [34,38,43] with and without an onset of infrared absorption in hydrogen at a critical temperature of ~3300 K (solid and dashed lines, respectively). Below the critical temperature (blue points), models (gray) are indistinguishable and follow behavior typical for a transparent sample with laser energy absorption on the foil surface [43]. For experiments achieving the critical temperature (red points), models (black) show the result of sample absorption: rather than an initial peak and decay that scaled with laser power, temperature is limited to values near the critical temperature [38]. Peak laser power increased from 65 to 155 W between the models. Above 100 GPa transient absorption occurred without this effect, since thinner samples at high pressure did not become infrared-optically thick when heated.

transition to the absorptive state. In this regime, hydrogen is heated directly by bulk absorption of laser energy, and this delocalization of heat energy compared to absorption at the foil surface limits the achievable temperature, giving rise to the plateau effect.

Transient absorption measurements (Fig. 2) confirm that the change in thermal history is correlated with increased optical absorption. Here, the absorption coefficient $\alpha = -\ln(I_H/I_C)/d$, where d is the thickness of the hot region (estimated from FE calculations, and of order 1 μm at 141 GPa), while I_C and I_H are transmitted probe intensities through cold and hot samples, respectively. Peak α near 1 μm^{-1} are consistently inferred, with total uncertainty of about an order of magnitude largely due to thickness uncertainty and reproducibility.

To compare our optical measurements in a wide, previously unexplored region of the phase diagram to prior data, we interpolated direct-current (dc) conductivity (σ_0) measurements on fluid hydrogen [3,11,12,29,35] using an experimentally consistent model [34] having the form $\sigma^* = \sigma_m^* - \sigma_j^*\{1 - 0.5\mathrm{erfc}[(T^* - T_c^*)/T_w^*]\}$, where $\sigma^* = \log(\sigma_0)$ and $T^* = 1/T$. This model has a sigmoidal temperature dependence that reproduces the Arrhenius-like or semiconductorlike proportionality of $\sigma^* \propto T^*$ during the IMT [11,12,29], with constant conductivity in purely metallic (σ_m^*) [13,14,29] and insulating ($\sigma_m^* - \sigma_j^*$) [35] states; the inverse transition temperature (T_c^*) and width (T_w^*) were taken to vary linearly with density [34].

Absorption spectra at 141 GPa and 2400 K show increasing absorption with photon energy across the visible [Fig. 4(a)]. Semiconductorlike absorption is one possible explanation: electronic band gaps on the order of the present optical energies have been reported in dense hydrogen [3,8,9,12,16,29,44,45]. The data do not permit the exact assignment to existing semiconductor or semimetal models. However, given the disordered nature of the material and rather large values of the absorption coefficients (up to ~10^6 m^{-1}), we suggest that observed absorption is due to optical processes between extended states, which are well described by Tauc's relation $\alpha = A(\hbar\omega - E_g)^2/\hbar\omega$. This well fits the data, implying a gap E_g of 0.9 ± 0.3 eV. In this semiconductor picture, hydrogen is electrically conductive due to thermal excitation of electrons. Assuming an effective carrier mass of $0.5 - 1\, m_e$ [13,38], the dc conductivity at these conditions is predicted to be 5–23 S/cm for $E_g = 0.9$ eV, in agreement with that determined from shock data (~15 S/cm) [46]. The spectral character is consistent with theory for semiconducting hydrogen at similar pressure and lower temperature [16], which may be similarly described by the Tauc model.

Conductivity at optical frequencies is $\sigma = n\alpha c\varepsilon_0$, where n is the real index of refraction [47,48], which is weakly dependent on material properties, and always of order 10^0 [34]. Thus, σ is determined principally by α, which varies by many orders of magnitude during electronic transformation. The conductivity at 2400 K and 141 GPa increases from ~70 to ~220 S/cm from 1.55 to 2.30 eV, and this extrapolated to zero energy is consistent with the dc conductivity of ~15 S/cm [Fig. 4(b)]. The decrease in conductivity with energy is inconsistent with the simple Drude model of free carriers widely used for hydrogen at extreme conditions [2,11–14,16,17].

A modified Drude model, after Smith [49], given by $\sigma = \sigma_0[1 + C(1 - \omega^2\tau^2)/(1 + \omega^2\tau^2)]/[(1 + C)(1 + \omega^2\tau^2)]$ and incorporating reduced electron mobility through a backscattering term C, does provide an adequate representation of the data including the dc limit [Fig. 4(b)]. This model has features typically observed in poor metals at the boundary of metallization transitions such as mercury [49] and argon [38], suggesting its applicability for hydrogen at the IMT. The parameter C, a measure of how closely the spectrum follows the Drude (free-electron) approximation, ranges from 0 to −1, with $C = 0$ (minimum backscattering) corresponding to the Drude form. Fits to our data show C is closer to −1 at conditions of incipient metallization [Fig. 4(c)]. This is consistent with theories for conducting hydrogen [17,21,23,24], which are well described by a Smith-Drude model with $C \neq 0$ [34]. Scattering times τ from Smith-Drude fits are insensitive to pressure and temperature [Fig. 4(d)] despite conditions sampled by experiment and theory ranging from 24 to 6000 GPa,

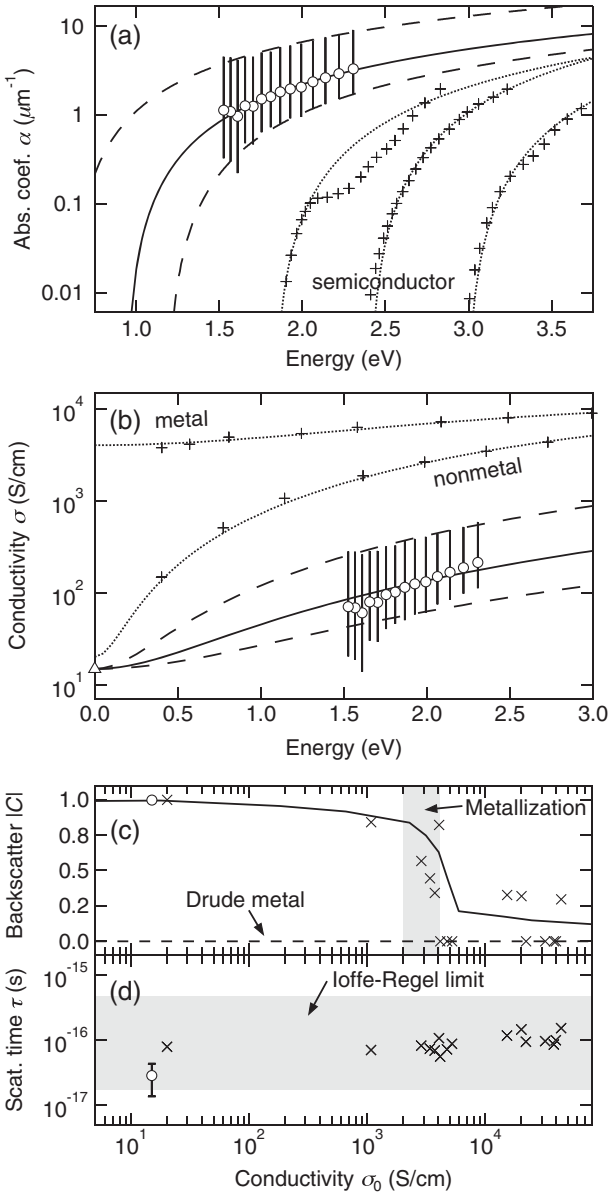

FIG. 4. Optical properties of hydrogen. Data at 141 GPa and 2400(300) K are open circles (error bars are systematic), theoretical predictions are crosses, and fits are lines. (a) Absorption spectra with Tauc fits, with theory for semiconducting states at 1600–1700 K, 101–159 GPa [16]. (b) Conductivity spectra with Smith-Drude fits. The dc conductivity corresponding to the present data and used in the fitting is $\sigma_0 = 15$ S/cm (triangle). Theory for metal and nonmetal states are for 1000 K, 170 GPa [21]. (c) Smith-Drude backscattering parameter C and (d) scattering time τ are from theory [17,21,23,24,34] and this experiment; shaded region in (c) is the conditions for metallization [12,21,29] and in (d) the calculated minimum scattering time (Ioffe-Regel limit) [12,13] for relevant conditions.

1000 to 125 000 K, and 0.3 to 5.4 g/cc [17,21,23,24], and are consistent with the expected minimum scattering time (Ioffe-Regel limit) [12,13] where scattering occurs at the interatomic spacing. Conductivity peaks at $\omega_m \approx 1/\tau$ when $C \approx -1$, or $\hbar\omega_m \approx 10$ eV for the present data. The fact that conduction is maximized in conjunction with the shortest-distance carrier motion possible suggests that transport is dominated by motion of bound carriers, such as hopping [18], as opposed to unimpeded long-distance flow.

The temperature at which absorbing hydrogen appears (at detection limit $\alpha \approx 0.1$ μm^{-1}) decreases weakly with pressure, remaining at 1700–2500 K at 30–110 GPa (Fig. 1). Here, $\sigma_0 \approx 10^{-3}$ S/cm, which is below the optical conductivity, $\sigma \approx 10^{0}$ S/cm. The data at 141 GPa and 2400 K have $\sigma_0 \approx 10^{1}$ S/cm, and $\sigma \approx 10^{2}$ S/cm at visible frequencies [Fig. 4(b)]. Fluid hydrogen thus shows optical properties characteristic of a weak metal [17,21,23,24] and a semiconductor [16] (σ increasing with frequency) throughout the observed pressure range at temperatures of 1700–2500 K. Measured optical conductivities (Fig. 4) are less than those of the metallic state (~2000 S/cm) [12,29], whereas optical reflectivity R, estimated by assessing the Fresnel reflectivity between insulating (cold) and optically transformed (hot) states in the experiment, is $R \approx [(4n\omega/\alpha c)^2 + 1]^{-1}$, or less than ~1% at presently examined conditions.

Our data directly show that hot fluid hydrogen retains a significant band gap to above 140 GPa pressure (Fig. 4) and temperatures of 2000–3000 K. Prior interpretations of conductivity data, assuming a density-dependent, temperature-independent gap, predicted metallization at these conditions (densities above 0.32 mol H_2/cc) via compressive gap closure [3,12,29]. The difference between our direct measurement and the prior model result is attributed to temperature dependence of the gap. Indeed, the temperature at which absorption appears in fluid hydrogen is nearly density- and pressure-independent between 30 and 110 GPa, suggesting that gap closure is primarily thermal rather than compressive.

The definitive observation of a weakly conducting, semiconductorlike state of hot fluid hydrogen in measurements to 150 GPa rules out the possibility of a rapid or first-order transformation between insulator and metal at these pressures. This is inconsistent with some *ab initio* theoretical predictions [5,19,21,22] and supports more recent theories employing nonlocal density functionals and nuclear quantum effects [25] or quantum Monte Carlo molecular dynamics [27], which place a critical point at 250–375 GPa. Isentropic compression experiments that find the IMT becomes first order by 285 GPa [16] suggest together with our results a critical point between 150 and 285 GPa. The gap in temperature between insulating and metallic states appears to be decreasing with pressure in the presently-studied range, consistent with the transition sharpening towards a critical point at higher pressures (Fig. 1): at 22 GPa, reflectivity [14] onsets 3710 K above absorption; at 45 GPa, the difference is 1540 K. Parallel behavior is seen in the dc conductivity (Fig. 1).

Prevailing first-principles models for hydrogen and hydrogen-bearing systems at high pressure and temperature in giant planets [4,5,50] thus require a significant reassessment. Compared with these theories, metallic conditions occur at higher pressure and temperature (i.e., deeper within the

planets), potentially influencing atmospheric coupling with the metallic layer [6,7] and the conditions of hydrogen-helium phase separation. For example, as conditions of phase separation are correlated with the location of the critical point [4,5,50], the increased pressure of the critical point required by our direct observations to 150 GPa suggests phase separation is unlikely to have occurred in Jupiter [34].

Our optical properties measurements on hydrogen cover a wide, previously unexplored region of the phase diagram and bridge large gaps between prior dynamic and static compression measurements of transformation and transport properties. Our data show the presence of an intermediate absorptive but not metallic state of hydrogen at the boundary between insulating and metallic regimes in the pressure range 10 to 150 GPa. This is inconsistent with the first-order insulator-metal transition and compression-driven gap closure that were previously inferred at these pressures from experiments and theory.

We thank S. Lobanov and M. Ahart for experimental assistance, C. T. Seagle, R. Boehler, and R. J. Hemley for helpful discussions, and R. T. Howie, V. Struzhkin, E. Gregoryanz, and three anonymous reviewers for constructive suggestions on this manuscript. This work was supported by the NSF Major Research Instrumentation program, NSF EAR-1015239, NSF EAR-1520648, and NSF EAR/IF-1128867, the Army Research Office (56122-CH-H), the Carnegie Institution of Washington, the Deep Carbon Observatory Instrumentation grant, the British Council Researcher Links program, the DOE NNSA Carnegie/DOE Alliance Center (DE-FC52-08NA28554), the EFree Energy Frontier Research Center funded by the U.S. Department of Energy Office of Science under Grant No. DE-SC0001057, and NSFC (No. 21473211).

*Corresponding author.
rs.mcwilliams@ed.ac.uk
†Corresponding author.
alex@issp.ac.cn

[1] N. W. Ashcroft, Metallic Hydrogen: A High-Temperature Superconductor?, Phys. Rev. Lett. **21**, 1748 (1968).
[2] S. X. Hu, L. A. Collins, V. N. Goncharov, T. R. Boehly, R. Epstein, R. L. McCrory, and S. Skupsky, First-principles opacity table of warm dense deuterium for inertial-confinement-fusion applications, Phys. Rev. E **90**, 033111 (2014).
[3] W. J. Nellis, S. T. Weir, and A. C. Mitchell, Metallization and electrical conductivity of hydrogen in Jupiter, Science **273**, 936 (1996).
[4] W. Lorenzen, B. Holst, and R. Redmer, Demixing of Hydrogen and Helium at Megabar Pressures, Phys. Rev. Lett. **102**, 115701 (2009).
[5] W. Lorenzen, B. Holst, and R. Redmer, Metallization in hydrogen-helium mixtures, Phys. Rev. B **84**, 235109 (2011).
[6] M. Heimpel and N. Gómez Pérez, On the relationship between zonal jets and dynamo action in giant planets, Geophys. Res. Lett. **38**, L14201 (2011).
[7] T. Gastine, J. Wicht, L. D. V. Duarte, M. Heimpel, and A. Becker, Explaining Jupiter's magnetic field and equatorial jet dynamics, Geophys. Res. Lett. **41**, 5410 (2014).
[8] P. Loubeyre, F. Occelli, and R. LeToullec, Optical studies of solid hydrogen to 320 GPa and evidence for black hydrogen, Nature (London) **416**, 613 (2002).
[9] R. T. Howie, C. L. Guillaume, T. Scheler, A. F. Goncharov, and E. Gregoryanz, Mixed Molecular and Atomic Phase of Dense Hydrogen, Phys. Rev. Lett. **108**, 125501 (2012).
[10] C.-s. Zha, Z. Liu, M. Ahart, R. Boehler, and R. J. Hemley, High-Pressure Measurements of Hydrogen Phase IV Using Synchrotron Infrared Spectroscopy, Phys. Rev. Lett. **110**, 217402 (2013).
[11] W. J. Nellis, A. C. Mitchell, P. C. McCandless, D. J. Erskine, and S. T. Weir, Electronic Energy Gap of Molecular Hydrogen From Electrical Conductivity Measurements at High Shock Pressures, Phys. Rev. Lett. **68**, 2937 (1992).
[12] W. J. Nellis, S. T. Weir, and A. C. Mitchell, Minimum metallic conductivity of fluid hydrogen at 140 GPa (1.4 Mbar), Phys. Rev. B **59**, 3434 (1999).
[13] P. M. Celliers, G. W. Collins, L. B. Da Silva, D. M. Gold, R. Cauble, R. J. Wallace, M. E. Foord, and B. A. Hammel, Shock-Induced Transformation of Liquid Deuterium into a Metallic Fluid, Phys. Rev. Lett. **84**, 5564 (2000).
[14] P. Loubeyre, S. Brygoo, J. Eggert, P. M. Celliers, D. K. Spaulding, J. R. Rygg, T. R. Boehly, G. W. Collins, and R. Jeanloz, Extended data set for the equation of state of warm dense hydrogen isotopes, Phys. Rev. B **86**, 144115 (2012).
[15] V. Dzyabura, M. Zaghoo, and I. F. Silvera, Evidence of a liquid-liquid phase transition in hot dense hydrogen, Proc. Natl. Acad. Sci. U.S.A. **110**, 8040 (2013).
[16] M. D. Knudson, M. P. Desjarlais, A. Becker, R. W. Lemke, K. R. Cochrane, M. E. Savage, D. E. Bliss, T. R. Mattsson, and R. Redmer, Direct observation of an abrupt insulator-to-metal transition in dense liquid deuterium, Science **348**, 1455 (2015).
[17] L. A. Collins, S. R. Bickham, J. D. Kress, S. Mazevet, T. J. Lenosky, N. J. Troullier, and W. Windl, Dynamical and optical properties of warm dense hydrogen, Phys. Rev. B **63**, 184110 (2001).
[18] R. Redmer, G. Röpke, S. Kuhlbrodt, and H. Reinholz, Hopping conductivity in dense hydrogen fluid, Phys. Rev. B **63**, 233104 (2001).
[19] S. Scandolo, Liquid–liquid phase transition in compressed hydrogen from first-principles simulations, Proc. Natl. Acad. Sci. U.S.A. **100**, 3051 (2003).
[20] S. A. Bonev, E. Schwegler, T. Ogitsu, and G. Galli, A quantum fluid of metallic hydrogen suggested by first-principles calculations, Nature (London) **431**, 669 (2004).
[21] M. A. Morales, C. Pierleoni, E. Schwegler, and D. M. Ceperley, Evidence for a first-order liquid-liquid transition in high-pressure hydrogen from ab initio simulations, Proc. Natl. Acad. Sci. U.S.A. **107**, 12799 (2010).
[22] I. Tamblyn and S. A. Bonev, Structure and Phase Boundaries of Compressed Liquid Hydrogen, Phys. Rev. Lett. **104**, 065702 (2010).
[23] S. Hamel, M. A. Morales, and E. Schwegler, Signature of helium segregation in hydrogen-helium mixtures, Phys. Rev. B **84**, 165110 (2011).
[24] L. A. Collins, J. D. Kress, and D. E. Hanson, Reflectivity of warm dense deuterium along the principal Hugoniot, Phys. Rev. B **85**, 233101 (2012).

[25] M. A. Morales, J. M. McMahon, C. Pierleoni, and D. M. Ceperley, Nuclear Quantum Effects and Nonlocal Exchange-Correlation Functionals Applied to Liquid Hydrogen at High Pressure, Phys. Rev. Lett. **110**, 065702 (2013).
[26] G. Mazzola, S. Yunoki, and S. Sorella, Unexpectedly high pressure for molecular dissociation in liquid hydrogen by electronic simulation, Nat. Commun. **5**, 3487 (2014).
[27] G. Mazzola and S. Sorella, Distinct Metallization and Atomization Transitions in Dense Liquid Hydrogen, Phys. Rev. Lett. **114**, 105701 (2015).
[28] R. T. Howie, P. Dalladay-Simpson, and E. Gregoryanz, Raman spectroscopy of hot hydrogen above 200 GPa, Nat. Mater. **14**, 495 (2015).
[29] S. T. Weir, A. C. Mitchell, and W. J. Nellis, Metallization of Fluid Molecular Hydrogen at 140 GPa (1.4 Mbar), Phys. Rev. Lett. **76**, 1860 (1996).
[30] J. H. Eggert, D. G. Hicks, P. M. Celliers, D. K. Bradley, R. S. McWilliams, R. Jeanloz, J. E. Miller, T. R. Boehly, and G. W. Collins, Melting temperature of diamond at ultrahigh pressure, Nat. Phys. **6**, 40 (2010).
[31] N. Subramanian, A. F. Goncharov, V. V. Struzhkin, M. Somayazulu, and R. J. Hemley, Bonding changes in hot fluid hydrogen at megabar pressures, Proc. Natl. Acad. Sci. U.S.A. **108**, 6014 (2011).
[32] A. F. Goncharov and J. C. Crowhurst, Raman Spectroscopy of Hot Compressed Hydrogen and Nitrogen: Implications for the Intramolecular Potential, Phys. Rev. Lett. **96**, 055504 (2006).
[33] A. F. Goncharov, J. C. Crowhurst, J. K. Dewhurst, S. Sharma, C. Sanloup, E. Gregoryanz, N. Guignot, and M. Mezouar, Thermal equation of state of cubic boron nitride: Implications for a high-temperature pressure scale, Phys. Rev. B **75**, 224114 (2007).
[34] See Supplemental Material at http://link.aps.org/supplemental/10.1103/PhysRevLett.116.255501 for supporting text, figures and data.
[35] W. L. Willis, Electrical conductivity of some cryogenic fluids, Cryogenics **6**, 279 (1966).
[36] N. Nettelmann, A. Becker, B. Holst, and R. Redmer, Jupiter models with improved ab-initio hydrogen equation of state, Astrophys. J. **750**, 52 (2012).
[37] N. Nettelmann, R. Pustow, and R. Redmer, Saturn layered structure and homogeneous evolution models with different EOSs, Icarus **225**, 548 (2013).
[38] R. S. McWilliams, D. A. Dalton, Z. Konopkova, M. F. Mahmood, and A. F. Goncharov, Opacity and conductivity measurements in noble gases at conditions of planetary and stellar interiors, Proc. Natl. Acad. Sci. U.S.A. **112**, 7925 (2015).
[39] H. K. Mao and R. J. Hemley, Ultrahigh-pressure transitions in solid hydrogen, Rev. Mod. Phys. **66**, 671 (1994).
[40] Y. Akahama and H. Kawamura, Diamond anvil Raman gauge in multimegabar pressure range, High Press. Res. **27**, 473 (2007).
[41] H. K. Mao, J. Xu, and P. M. Bell, Calibration of the ruby pressure gauge to 800 kbar under quasi-hydrostatic conditions, J. Geophys. Res. **91**, 4673 (1986).
[42] T. Scheler, M. Marques, Z. Konopkova, C. L. Guillaume, R. T. Howie, and E. Gregoryanz, High-Pressure Synthesis and Characterization of Iridium Trihydride, Phys. Rev. Lett. **111**, 215503 (2013).
[43] J. A. Montoya and A. F. Goncharov, Finite element calculations of the time dependent thermal fluxes in the laser-heated diamond anvil cell, J. Appl. Phys. **111**, 112617 (2012).
[44] C.-S. Zha, Z. Liu, and R. J. Hemley, Synchrotron Infrared Measurements of Dense Hydrogen to 360 GPa, Phys. Rev. Lett. **108**, 146402 (2012).
[45] A. F. Goncharov, J. S. Tse, H. Wang, J. Yang, V. V. Struzhkin, R. T. Howie, and E. Gregoryanz, Bonding, structures, and band gap closure of hydrogen at high pressures, Phys. Rev. B **87**, 024101 (2013).
[46] dc conductivity is taken from the lower end of the temperature range achieved at this laser power, since the stacked transient absorption data (Fig. 2) are dominated by those cycles reaching lower temperature and lower absorption.
[47] W. J. Evans and I. F. Silvera, Index of refraction, polarizability, and equation of state of solid molecular hydrogen, Phys. Rev. B **57**, 14105 (1998).
[48] R. J. Hemley, M. Hanfland, and H. K. Mao, High-pressure dielectric measurements of solid hydrogen to 170 GPa, Nature (London) **350**, 488 (1991).
[49] N. V. Smith, Classical generalization of the Drude formula for the optical conductivity, Phys. Rev. B **64**, 155106 (2001).
[50] M. A. Morales, S. Hamel, K. Caspersen, and E. Schwegler, Hydrogen-helium demixing from first principles: From diamond anvil cells to planetary interiors, Phys. Rev. B **87**, 174105 (2013).